Supplementary Discussion

An unexpected second binding site for GSH

In addition to the GSH molecules in the central cavity, we observed an additional GSH inserted between TM 7'/8' of one monomer and TM 9/10 of the other (Fig. 4A, Supplementary Fig. S13A). This unexpected GSH wedge is held in place by a set of hydrogen bonds and ionic interactions. The central cysteine in the GSH interacts with the side chains of D374' and R450, and the carboxyl group of the C-terminal glycine interacts with the side chains of E346' and Y476. In contrast, the N-terminal glutamate residue points away from the protein, and does not create essential intermolecular interactions. Structure comparison indicated that binding of the GSH wedge just affected the local structure of D374, which is rotated by ~60 degrees (Supplementary Fig. S13B). Although the nonspecific effect of amino acid substitutions cannot be fully excluded, the single (D374A) and quadruple mutation (E346A/D374A/Y476A/R540A) showed reduced basal and maximum catalytic activity (Supplementary Fig. S13C). However, the stimulation levels of the mutants were still quite high, suggesting that the observed GSH wedge in the structure may not be essential for protein function. Interestingly, similar structural feature was also observed in the ABC exporter *Na*Atm1, a bacterial homologue of the human ABCB6 and ABCB7 transporters, in which the detergent molecule used for purification was inserted into the hydrophobic interface between the two TM halves (Supplementary Fig. S13D) (Lee et al., 2014).

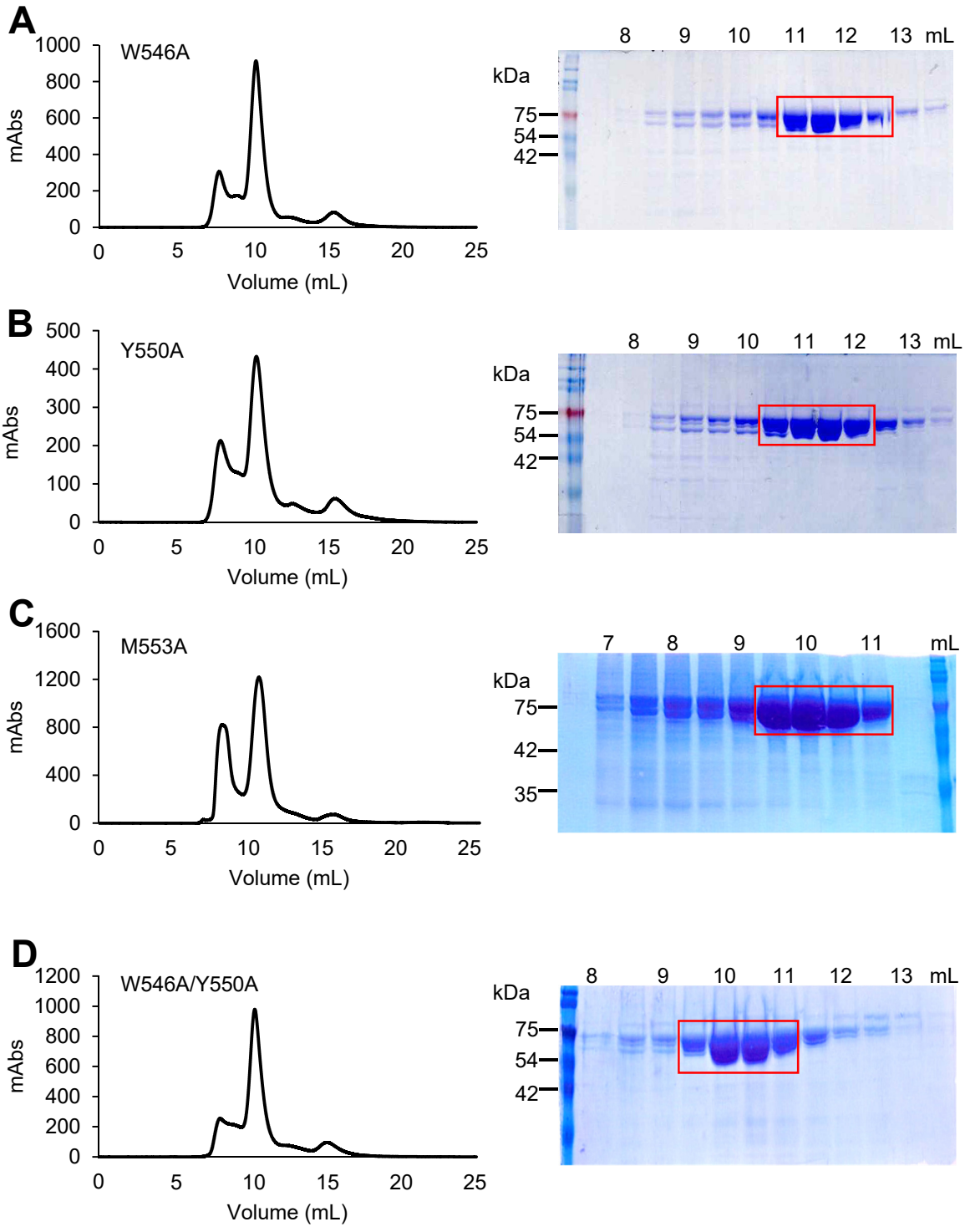
A
W546A
mAbs
Volume (mL)
kDa
75
54
42
8 9 10 11 12 13 mL
B
Y550A
mAbs
Volume (mL)
kDa
75
54
42
8 9 10 11 12 13 mL
C
M553A
mAbs
Volume (mL)
kDa
75
42
35
7 8 9 10 11 mL
D
W546A/Y550A
mAbs
Volume (mL)
kDa
75
54
42
8 9 10 11 12 13 mL

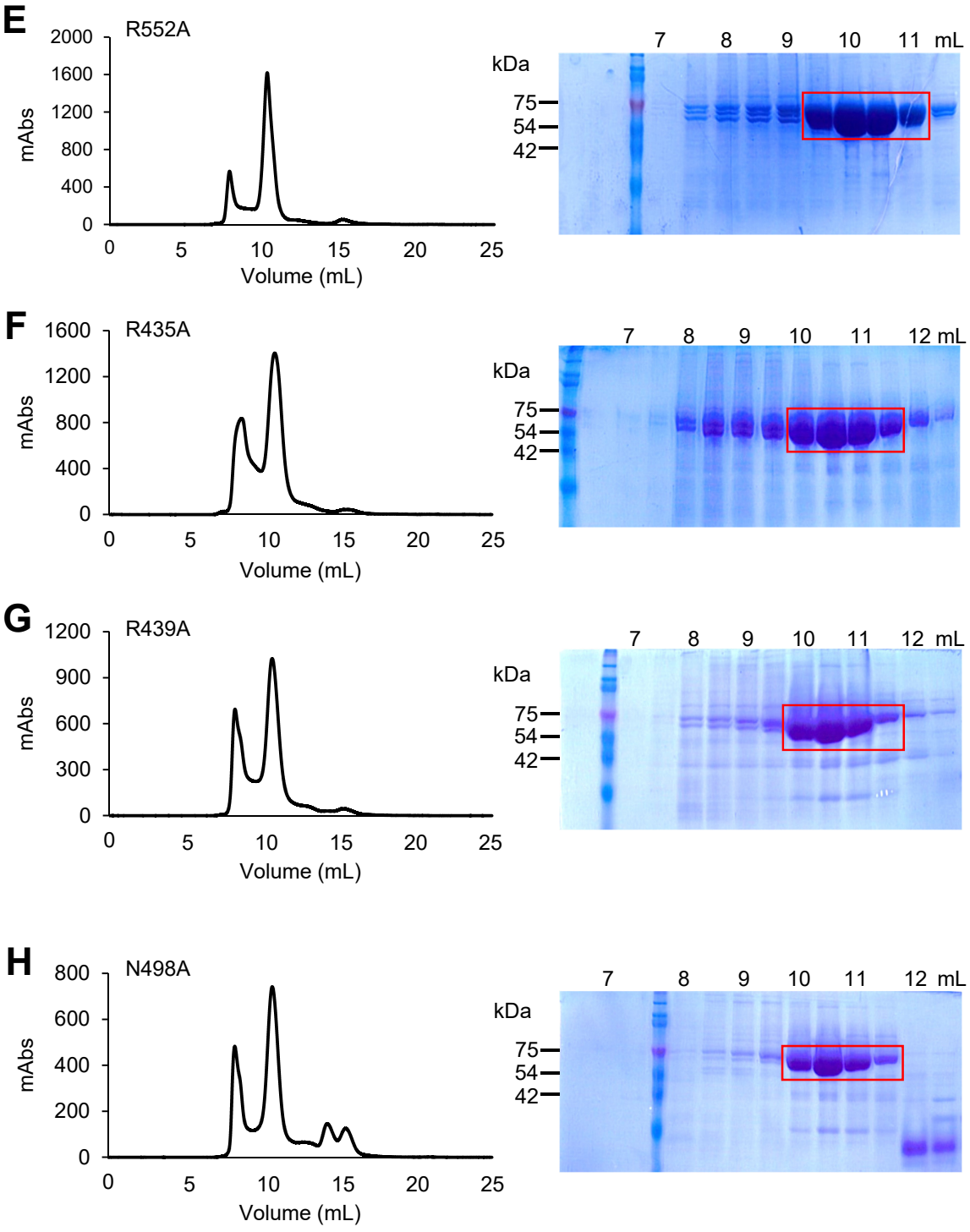
E
R552A
mAbs
2000
1600
1200
800
400
0
0 5 10 15 20 25
Volume (mL)
kDa
75
54
42
7 8 9 10 11 mL
F
R435A
mAbs
1600
1200
800
400
0
0 5 10 15 20 25
Volume (mL)
kDa
75
54
42
7 8 9 10 11 12 mL
G
R439A
mAbs
1200
900
600
300
0
0 5 10 15 20 25
Volume (mL)
kDa
75
54
42
7 8 9 10 11 12 mL
H
N498A
mAbs
800
600
400
200
0
0 5 10 15 20 25
Volume (mL)
kDa
75
54
42
7 8 9 10 11 12 mL

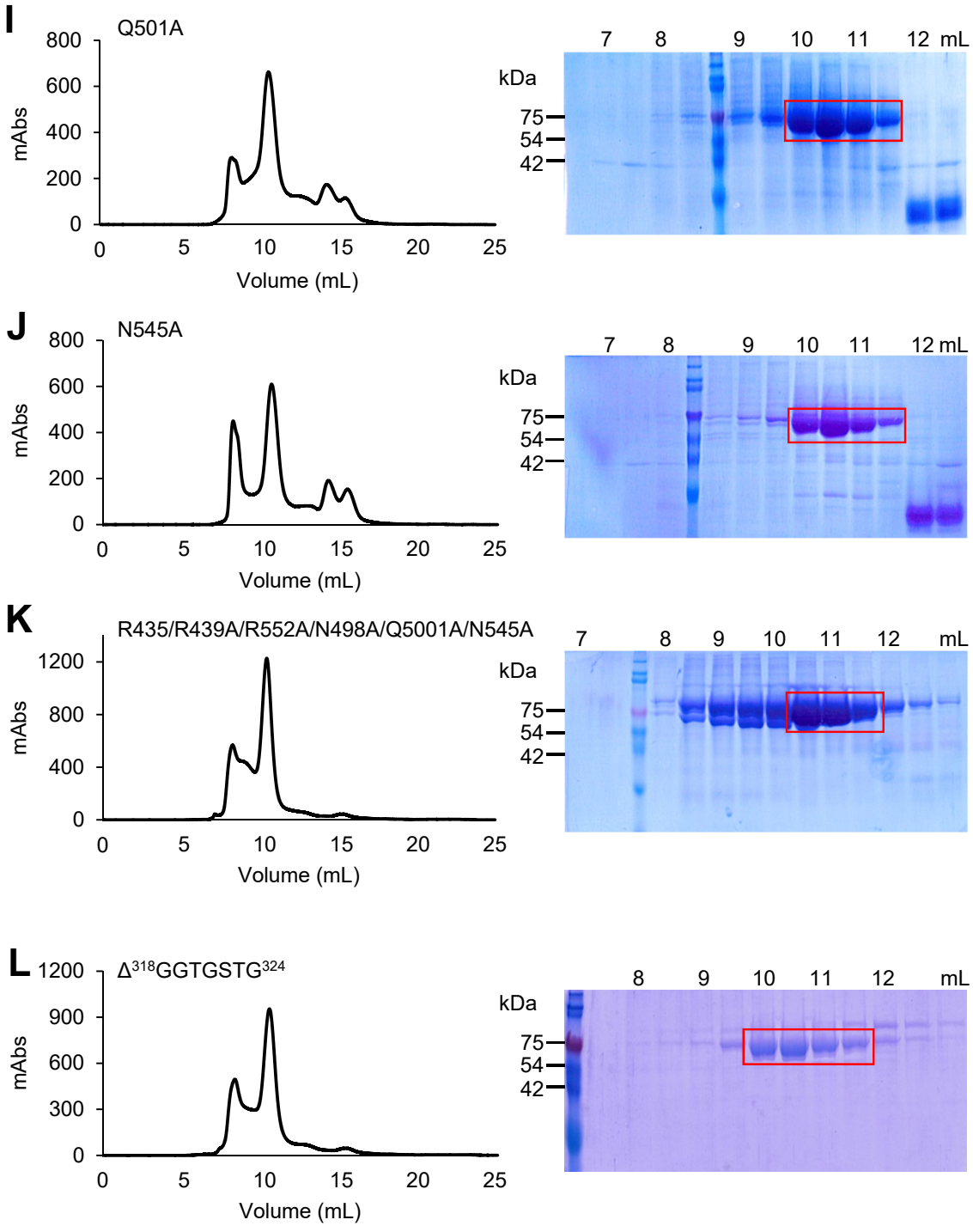
I
Q501A
mAbs
800
600
400
200
0
0
5
10
15
20
25
Volume (mL)
7
8
9
10
11
12
mL
kDa
75
54
42
J
N545A
mAbs
800
600
400
200
0
0
5
10
15
20
25
Volume (mL)
7
8
9
10
11
12 mL
kDa
75
54
42
K
R435/R439A/R552A/N498A/Q5001A/N545A
mAbs
1200
800
400
0
0
5
10
15
20
25
Volume (mL)
7
8
9
10
11
12
mL
kDa
75
54
42
L
Δ318GGTGSTG324
mAbs
1200
900
600
300
0
0
5
10
15
20
25
Volume (mL)
8
9
10
11
12
mL
kDa
75
54
42

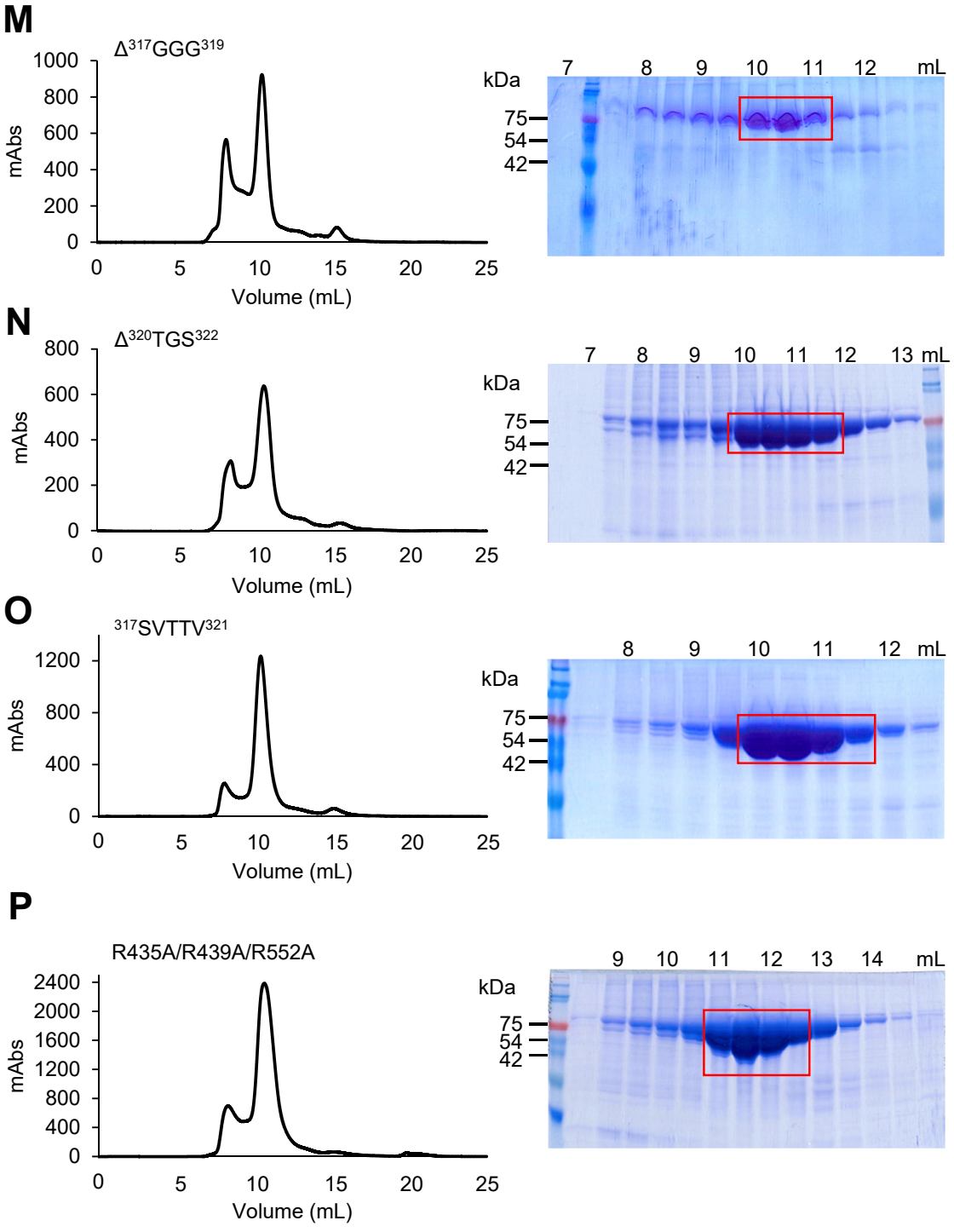
M
Δ317GGG319
mAbs
Volume (mL)
kDa
75
54
42
7 8 9 10 11 12 mL
N
Δ320TGS322
mAbs
Volume (mL)
kDa
75
54
42
7 8 9 10 11 12 13 mL
O
317SVTTV321
mAbs
Volume (mL)
kDa
75
54
42
8 9 10 11 12 mL
P
R435A/R439A/R552A
mAbs
Volume (mL)
kDa
75
54
42
9 10 11 12 13 14 mL

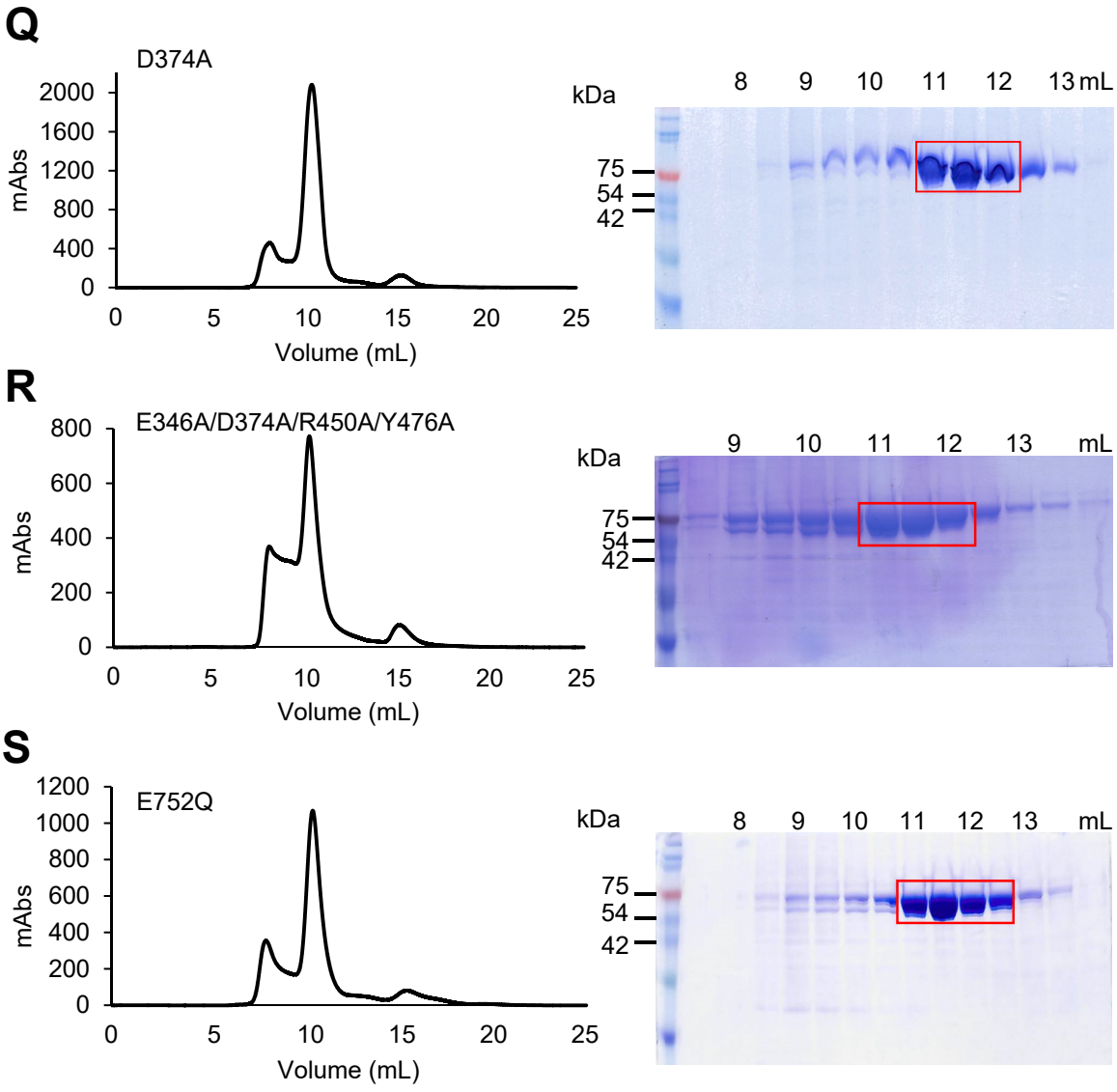

Supplementary Fig. S1. Elution profiles from size exclusion chromatography of the mutant proteins used in this study, and the results of SDS-PAGE. The pooled fractions are boxed in red.

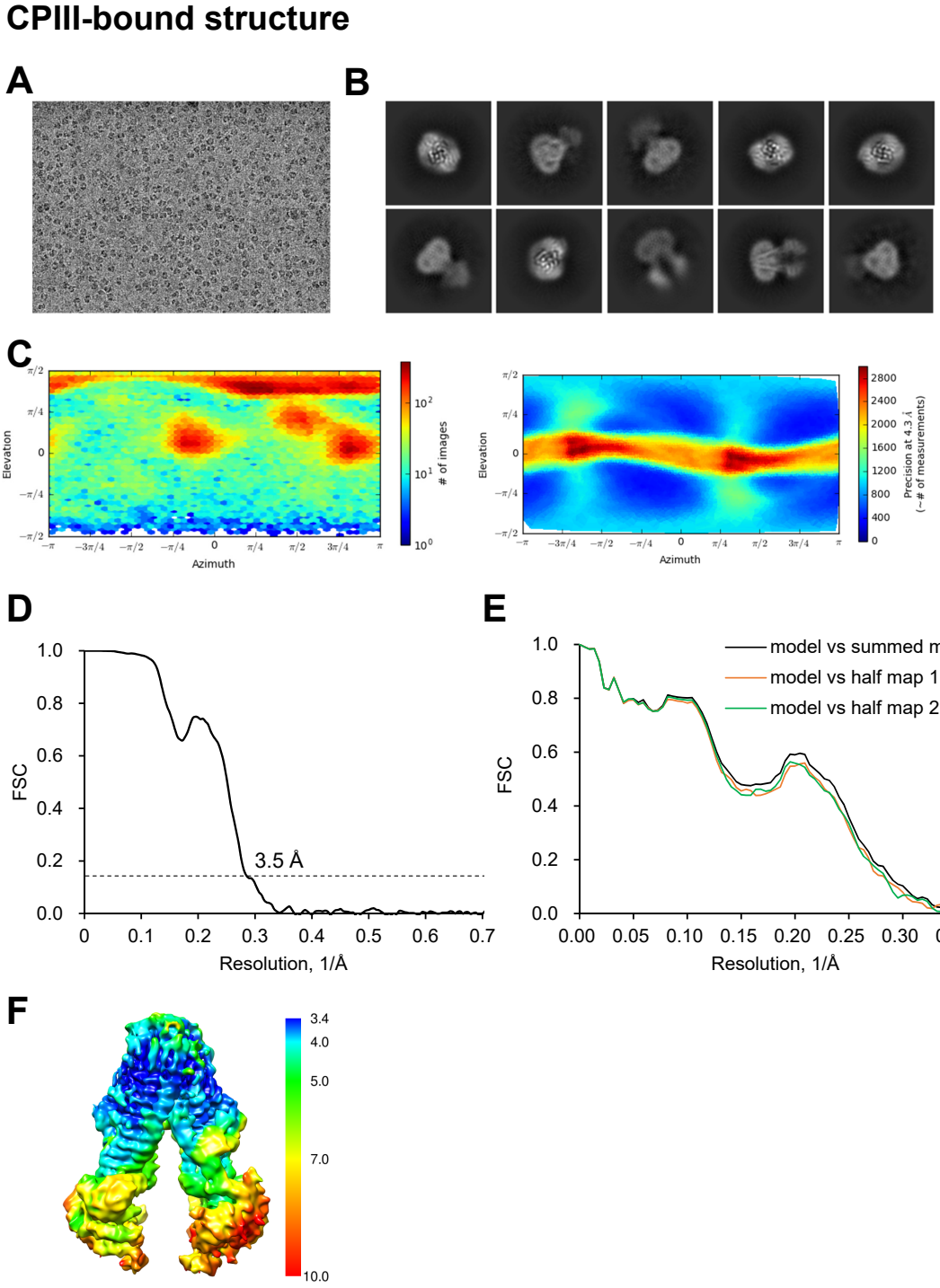

Supplementary Fig. S2. Cryo-EM analysis of CPIII-bound ABCB6-ΔTMD0. (A) Drift-corrected, dose-weighted micrograph. (B) Representative 2D class averages for the dataset. (C) Angular distribution plot for the final reconstruction. Heat map calculated in cryoSPARC shows number of particles for each viewing angle (red means more, blue means less). (D) The Gold Standard Fourier Shell Correlation (GSFSC) from cryoSPARC. The dashed line represents the 0.143 FSC cutoff criterion. (E) FSCs calculated between the refined structure and the half map used for refinement (work), the other half map (free) and the full map. (F) Local resolution map calculated by cryoSPARC.

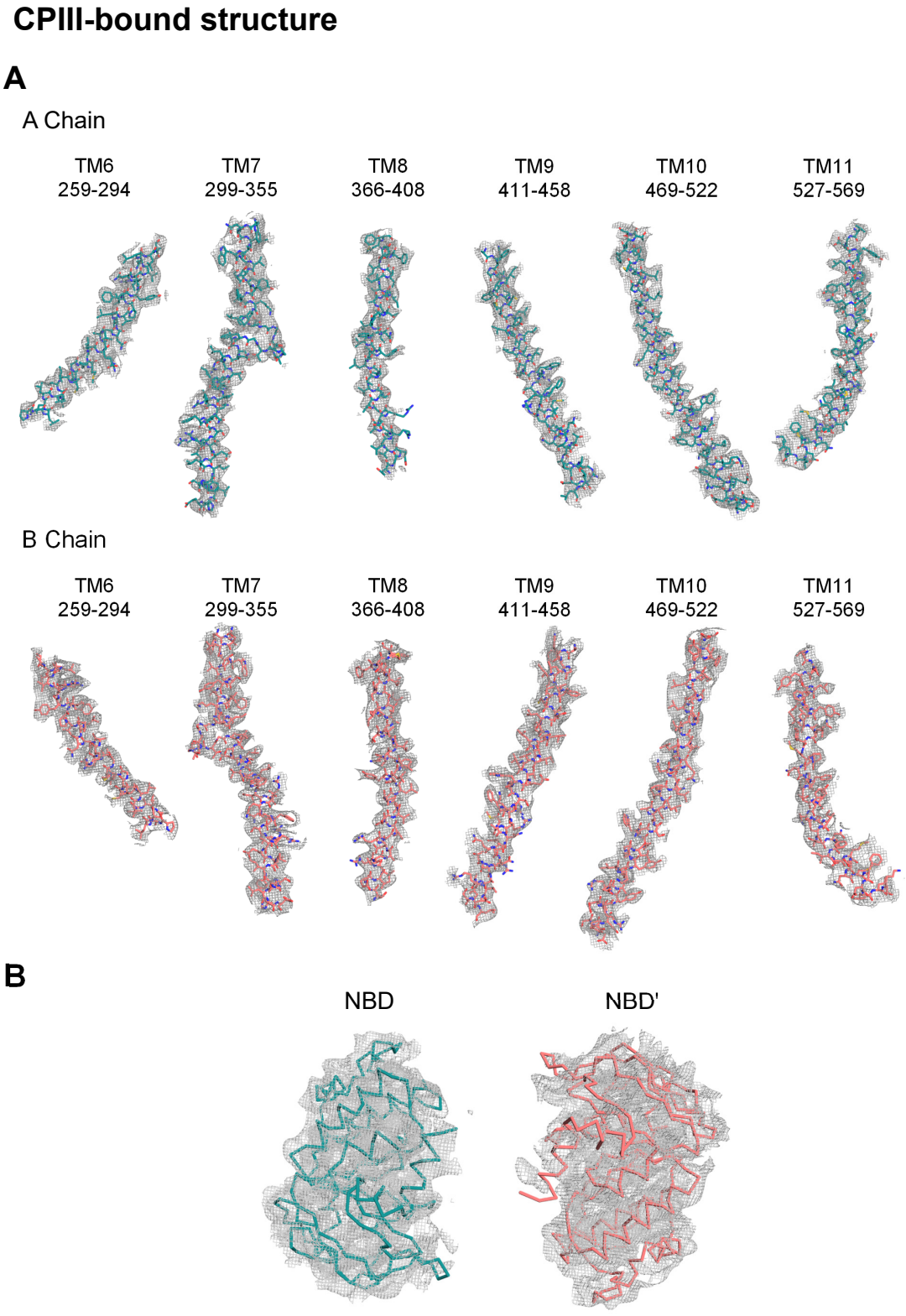

Supplementary Fig. S3. B-factor-sharpened EM maps of TM helices and NBDs in CPIII-bound ABCB6-ΔTMD0.

CPIII-bound structure

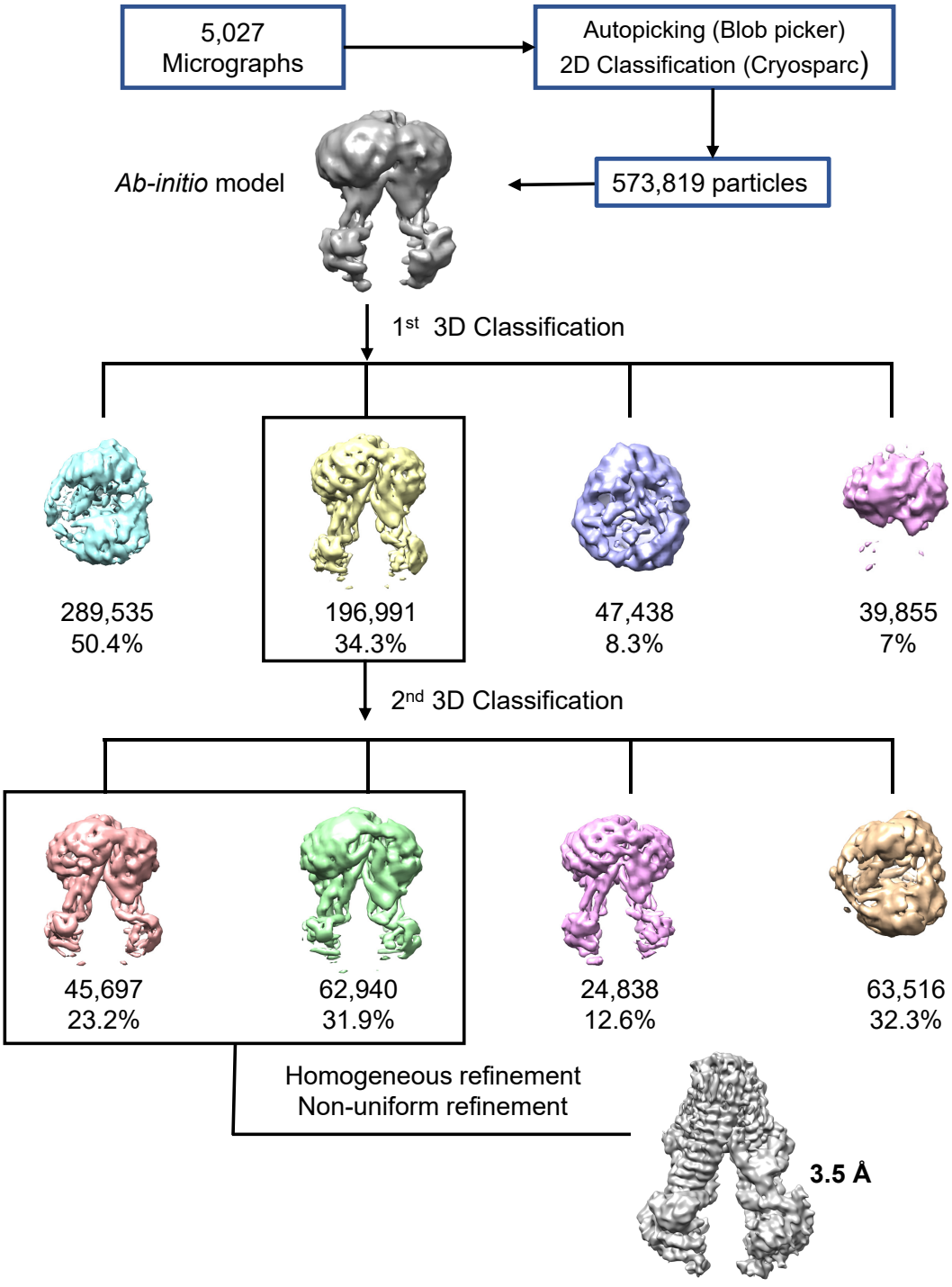

Supplementary Fig. S4. Cryo-EM data processing of CPIII-bound ABCB6-ΔTMD0.

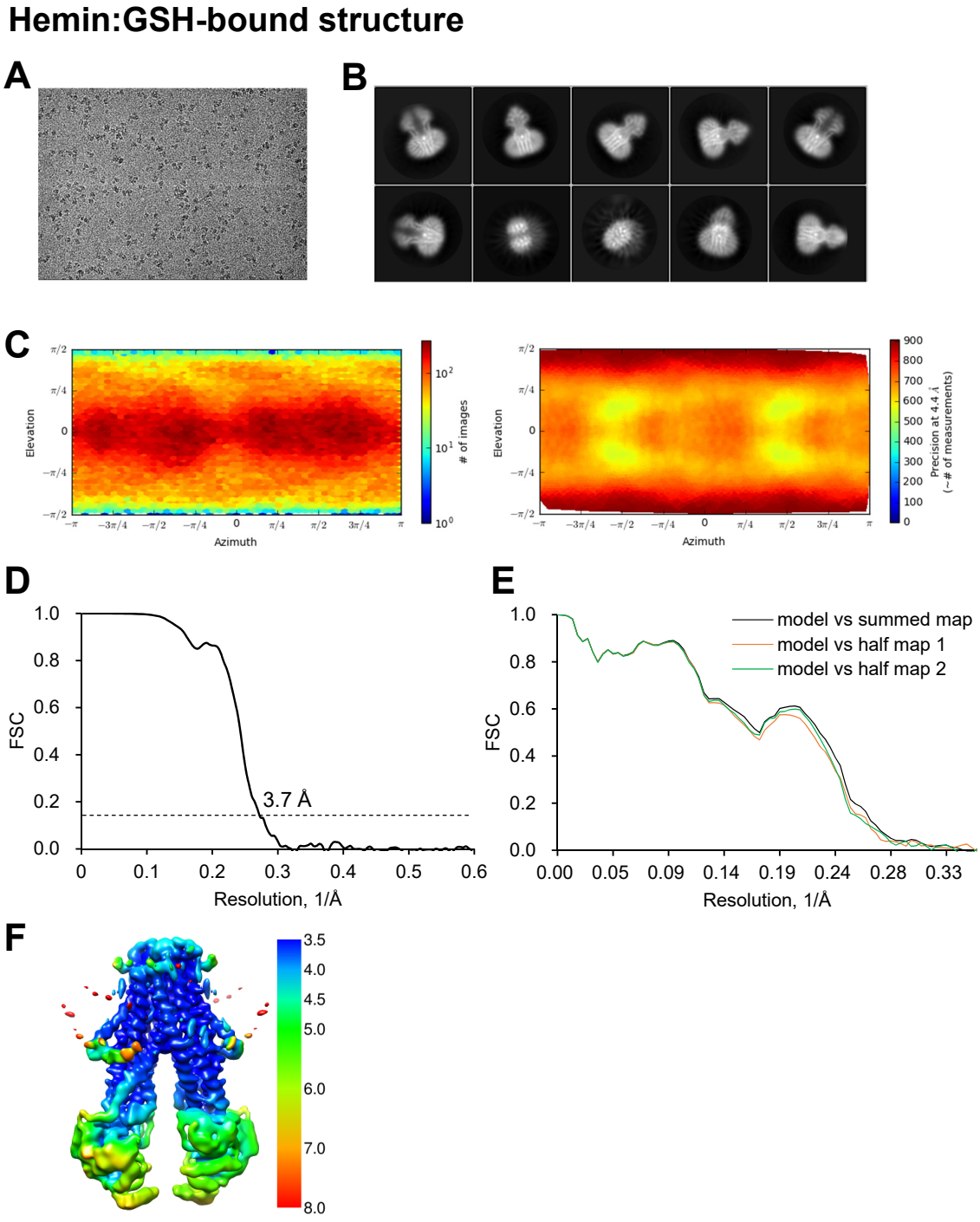

Supplementary Fig. S5. Cryo-EM analysis of ABCB6-ΔTMD0 in complex with hemin and GSH. (A) Drift-corrected, dose-weighted micrograph. (B) Representative 2D class averages for the dataset. (C) Angular distribution plot for the final reconstruction. Heat map calculated in cryoSPARC shows the number of particles for each viewing angle (red means more, blue means less). (D) The Gold Standard Fourier Shell Correlation (GSFSC) from cryoSPARC. The dashed line represents the 0.143 FSC cutoff criterion. (E) FSCs calculated between the refined structure and the half map used for refinement (work), the other half map (free) and the full map. (F) Local resolution map calculated by cryoSPARC.

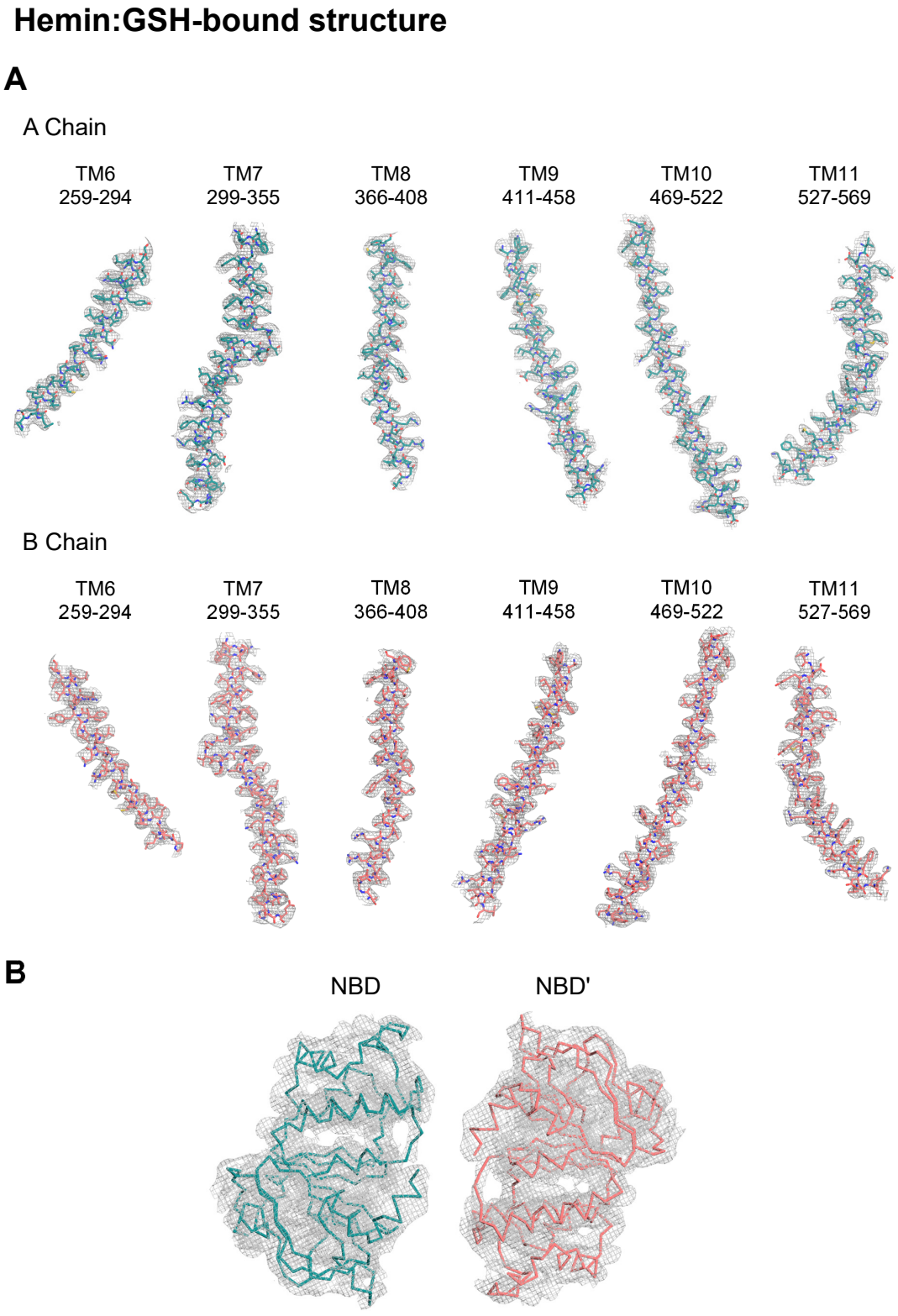

Supplementary Fig. S6. B-factor-sharpened EM maps of ABCB6-ΔTMD0 in complex with hemin and GSH.

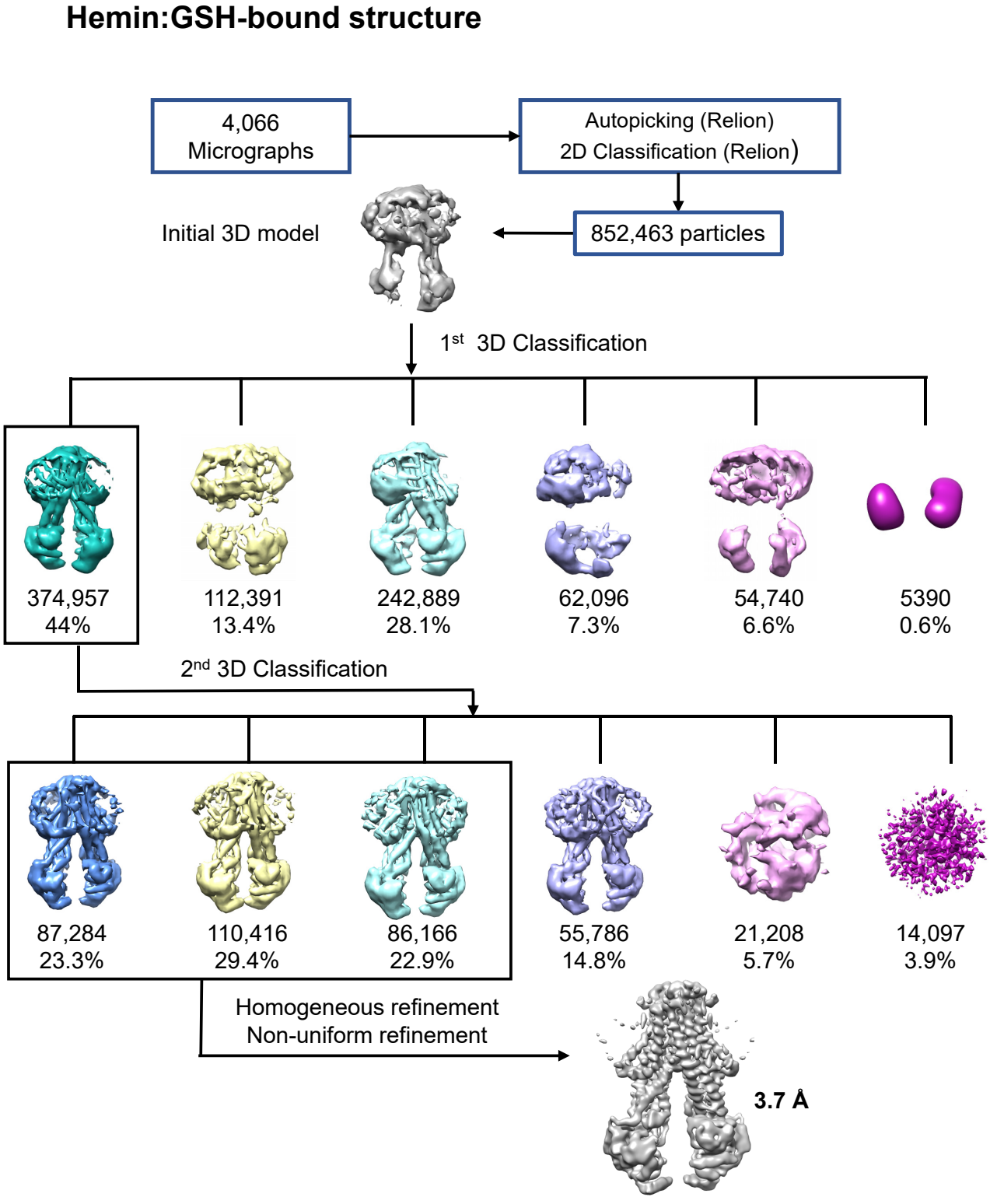

Supplementary Fig. S7. Cryo-EM data processing of ABCB6-ΔTMD0 in complex with hemin and GSH.

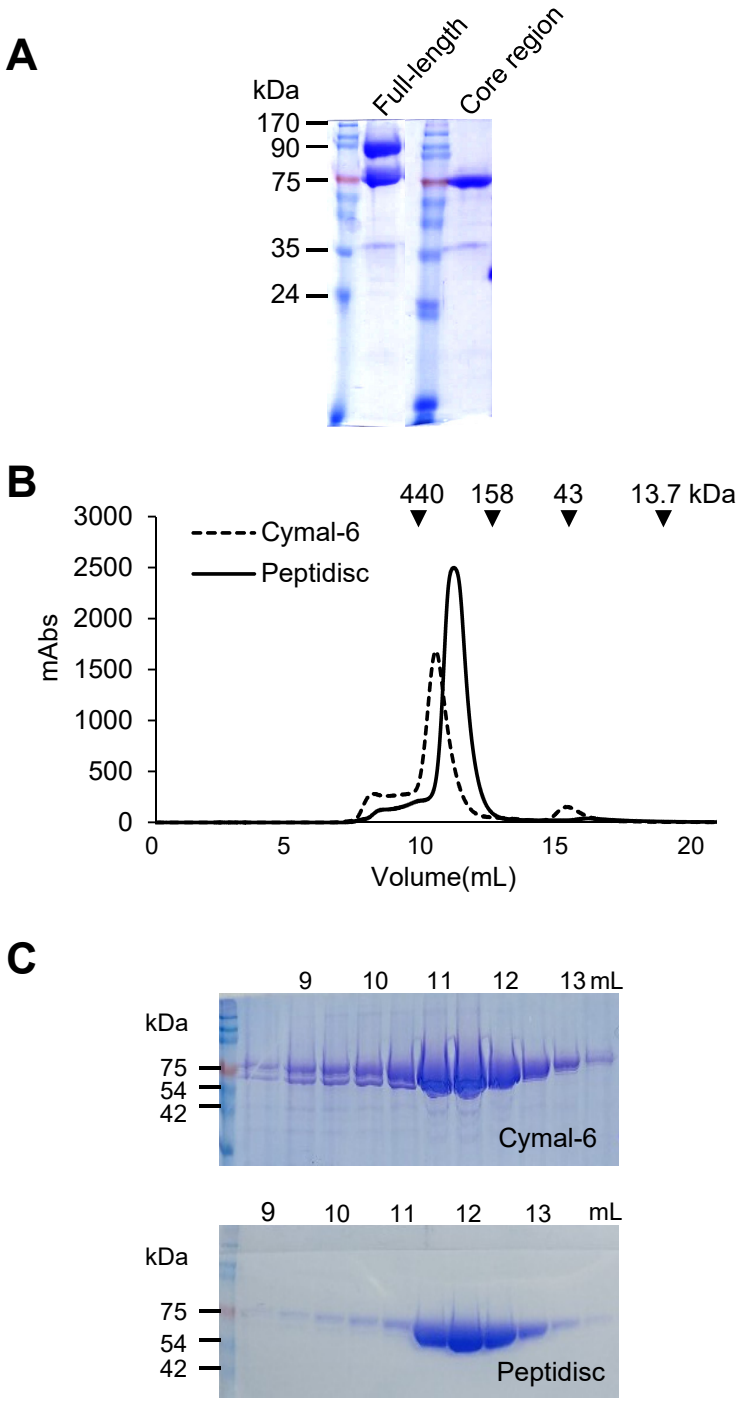

Supplementary Fig. S8. Purification and gel filtration analysis of proteins. (A) SDS-PAGE analysis of full-length ABCB6 (residues 1-842) and its core region (ABCB6-ΔTMD0, residues 206-842) after purification. (B) Elution profile of ABCB6-ΔTMD0 in detergent (dashed line) or peptidisc (solid line) using a Superdex Increase 200 10/300 GL column. The triangles represent the molecular weight positions of gel filtration standards, ferritin (440 kDa), aldolase (158 kDa), ovalbumin (43 kDa), and ribonuclease A (13.7 kDa). (C) SDS-PAGE analyses of ABCB6-ΔTMD0 purified in detergent (top) and peptidisc (bottom).

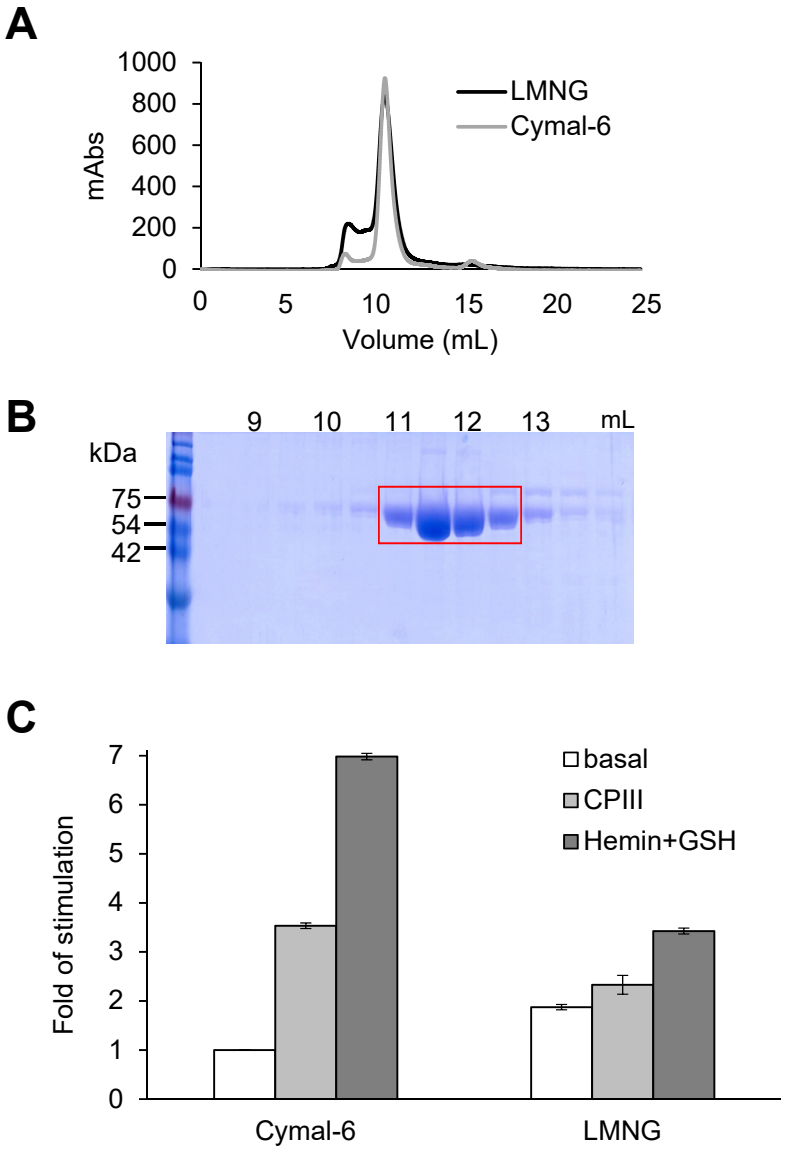

Supplementary Fig. S9. The ATPase activities of ABCB6-ΔTMD0 purified in different detergents. (A) Elution profiles of ABCB6-ΔTMD0 in LMNG (black line) or Cymal-6 (gray line) using a Superdex Increase 200 10/300 GL column. (B) SDS-PAGE analysis of ABCB6-ΔTMD0 purified in LMNG. (C) ATPase activity of ABCB6-ΔTMD0 in the presence of 50 μM CPIII, 10 μM hemin and 1 mM GSH. The basal activity of ABCB6-ΔTMD0 in Cymal-6 is set at 100%. Data points represent means ± standard deviations of three independent experiments.

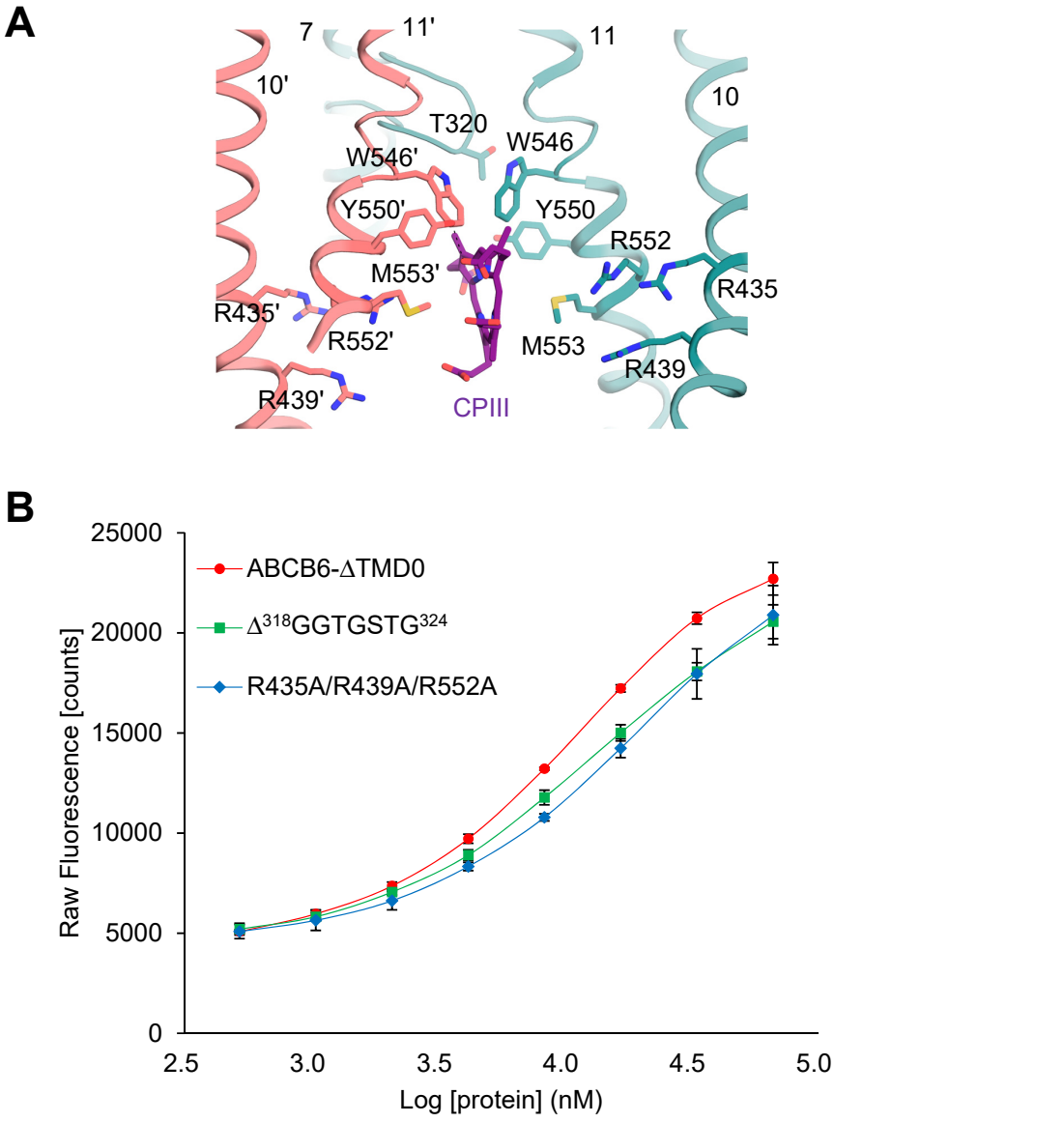

Supplementary Fig. S10. Measurement of the dissociation constant (K_d) of CPIII. (A) Relative positions of the positively charged arginine residues (R435, R439 and R552) in the CPIII binding site are shown. (B) Binding affinities of proteins to CPIII based on MST analysis (initial fluorescence). The ABCB6-ΔTMD0 protein has higher fluorescence enhancement than the two mutants when binding CPIII molecules. Each point is the mean ± SD of three measurements.

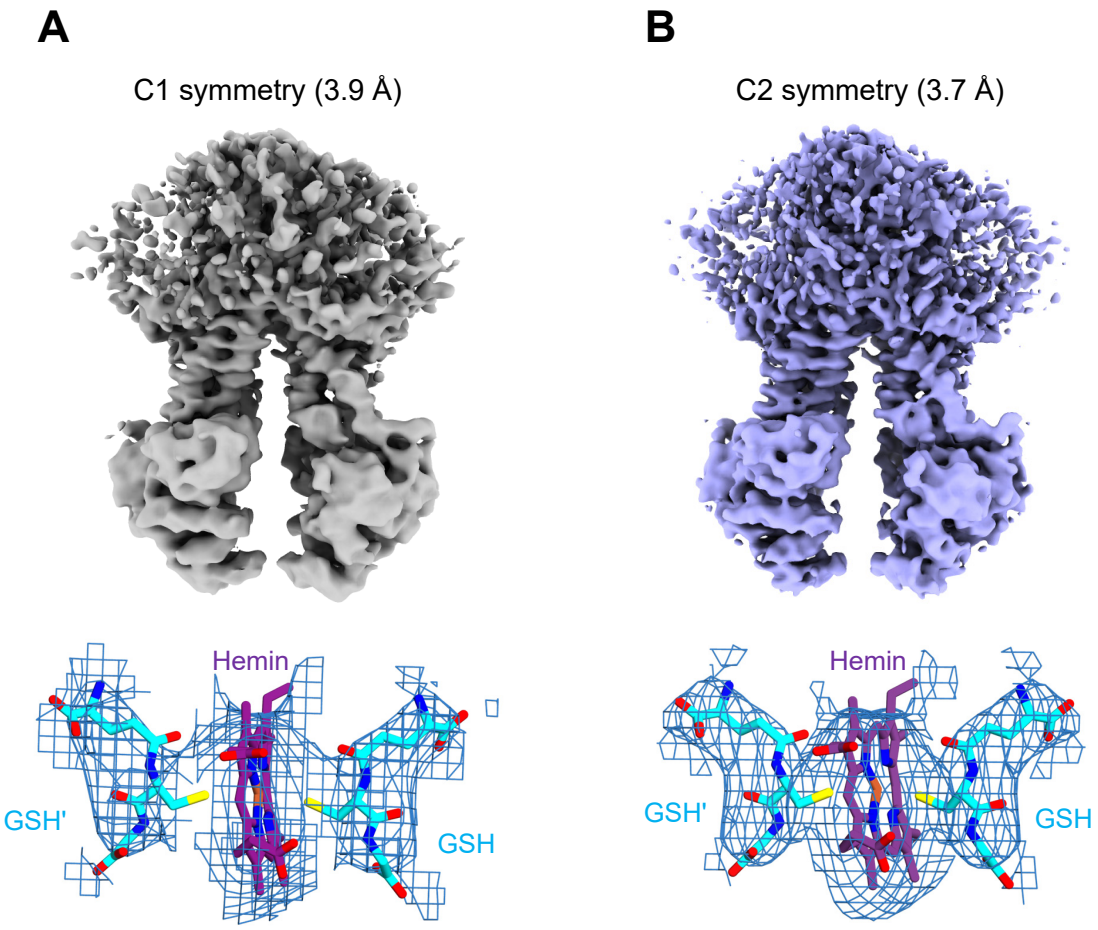

Supplementary Fig. S11. Comparison of cryo-EM density maps of hemin:GSH-bound structures produced by applying C1 and C2 symmetry. (A) The C1 symmetry cryo-EM map and the refined atomic coordinates of hemin and GSH. (B) The C2 symmetry cryo-EM map and the refined atomic coordinates of hemin and GSH. There was no difference in the overall structure observed, but there was a slight improvement in the resolution of the substrate binding site when C2 symmetry was imposed. The EM density of hemin and GSH is shown at 4 σ level.

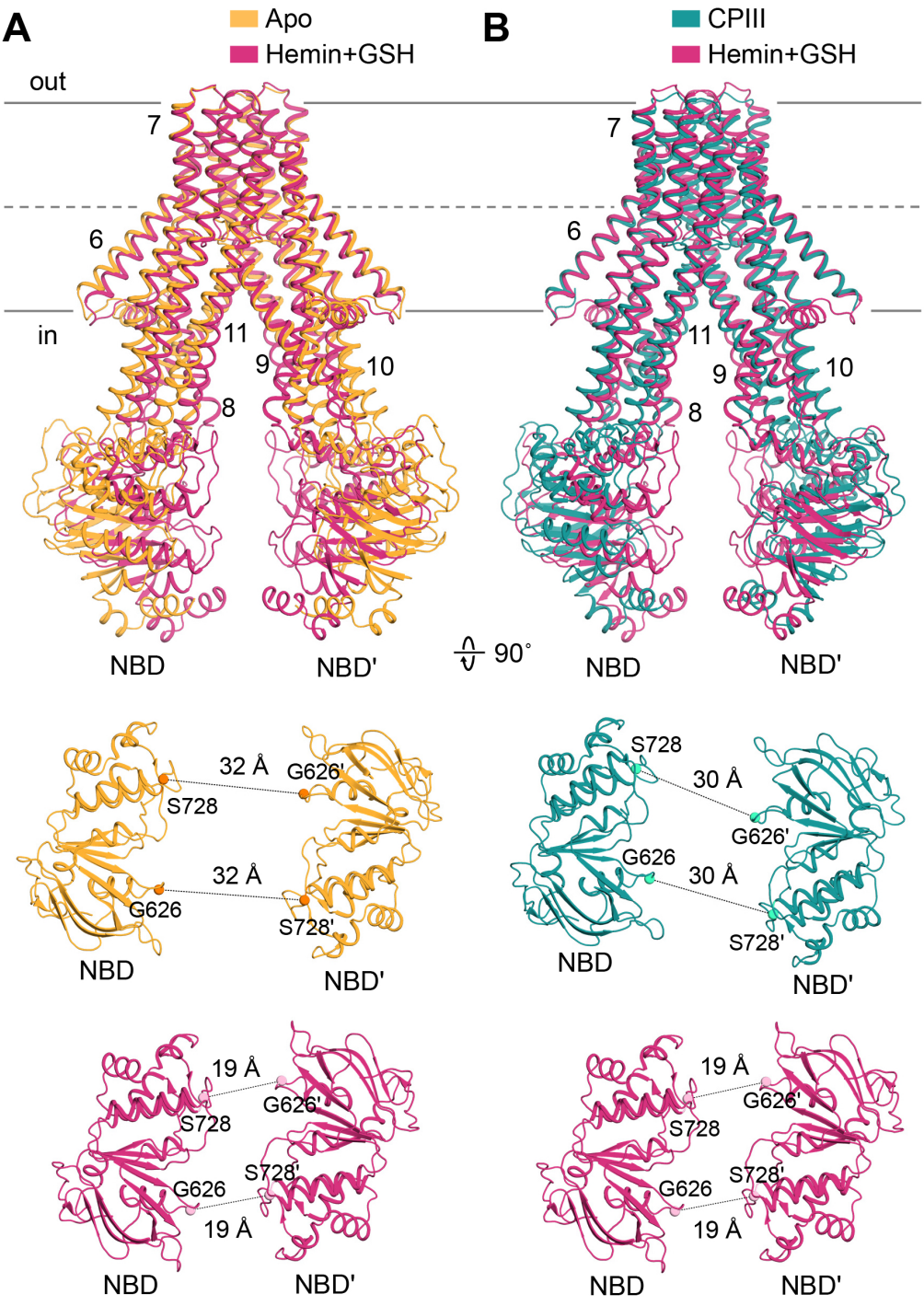

Supplementary Fig. S12. Structure comparison of ABCB6-ΔTMD0 with and without porphyrins. (A) The apo (PDB ID 7D7R) and hemin:GSH-bound structures are aligned. The Cα distances between the conserved G626 of the Walker A motif and the S728 of the signature motif is indicated. (B) The CPIII- and hemin:GSH-bound structures are aligned.

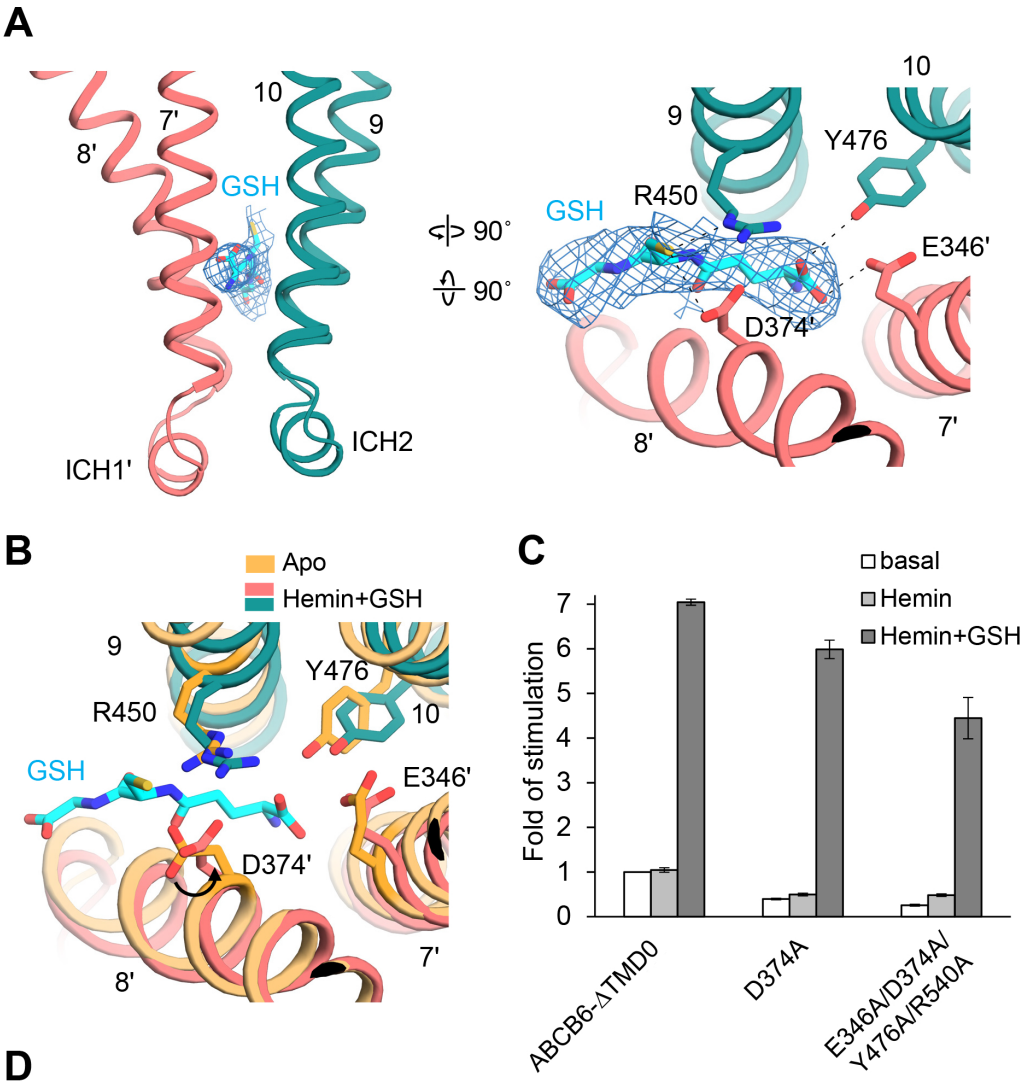

Supplementary Fig. S13. The GSH binding site between TM helices 7'/8' and 9/10 in ABCB6-ΔTMD0. (A) The EM density of the GSH molecule embedded in the TM helices is shown at the 3 σ level. Related to Figure 4A. (B) Comparison of the side chains lining the GSH wedge-binding site. The change of D374 structure is marked by a black arrow. (C) ATPase activity of the ABCB6-ΔTMD0 variants with 10 μM hemin in the presence or absence of 1 mM GSH. The basal activity of the wild-type is set at 100%. Data are means±SD of triplicate measurements. (D) The detergent (LDAO; Lauryldimethylamine Oxide) binding site between TM helices 4/5 and 2'/3' in *Na*Atm1 from *Novosphingobium aromaticivorans* DSM 12444 (PDB ID 4MRN).

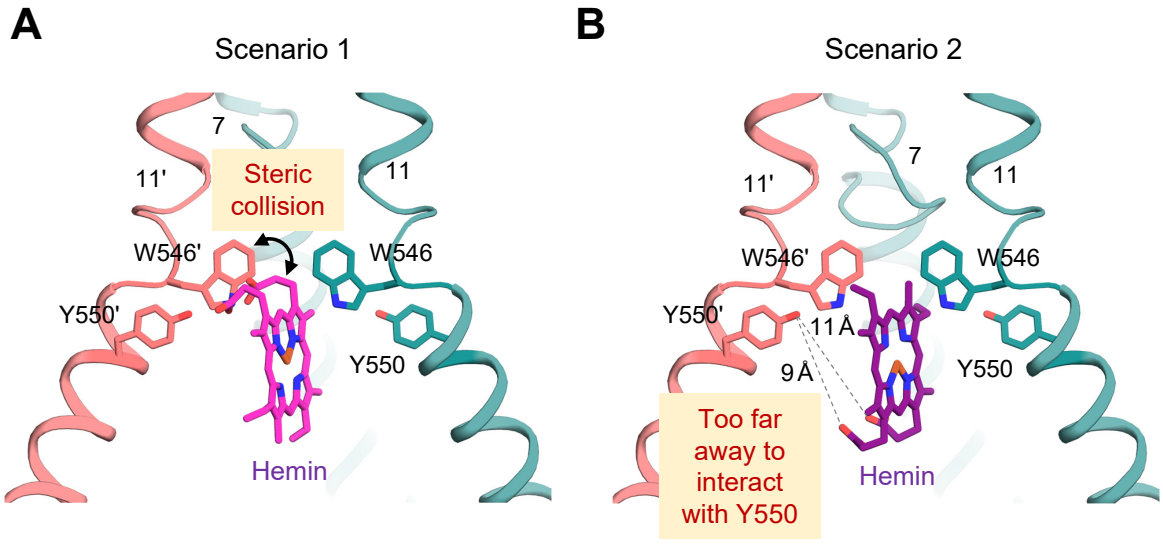

Supplementary Fig. S14. The nonproductive binding modes of hemin. (A) If the propionate group of hemin points upward (scenario 1), it causes severe steric clashes with the W546 residue. The GSHs are omitted for simplicity. (B) If it points downward (scenario 2), it can avoid steric clashes with neighboring residues. However, this binding mode prevents the hemin propionate group from interacting with Y550.

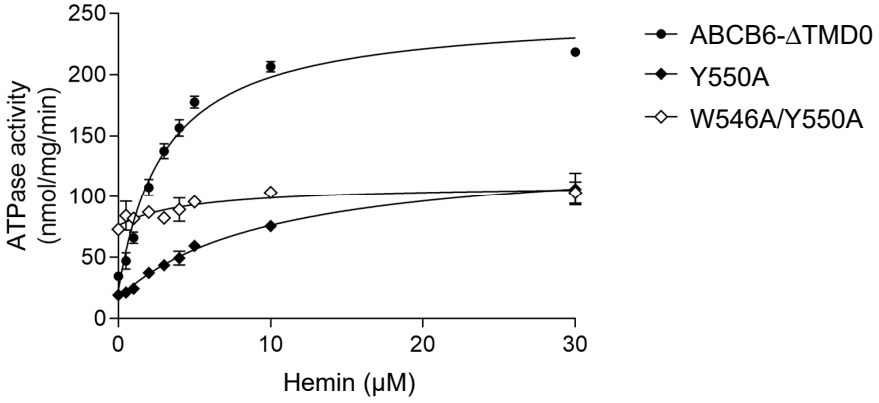

Supplementary Fig. S15. ATPase activity of the ABCB6-ΔTMD0 variants as a function of hemin concentration. ATPase activity of the ABCB6-ΔTMD0 variants as a function of hemin concentration in the presence of 1 mM GSH. The K_m value of Y550A for hemin was found to be 10 ± 1.3 μM and maximal ATPase activity was 136 ± 6 nmol/mg/min (or 19 min^{-1}). Data for the ABCB6-ΔTMD0 are the same as in Figure 1D. Data points represent the mean±SD of three measurements.

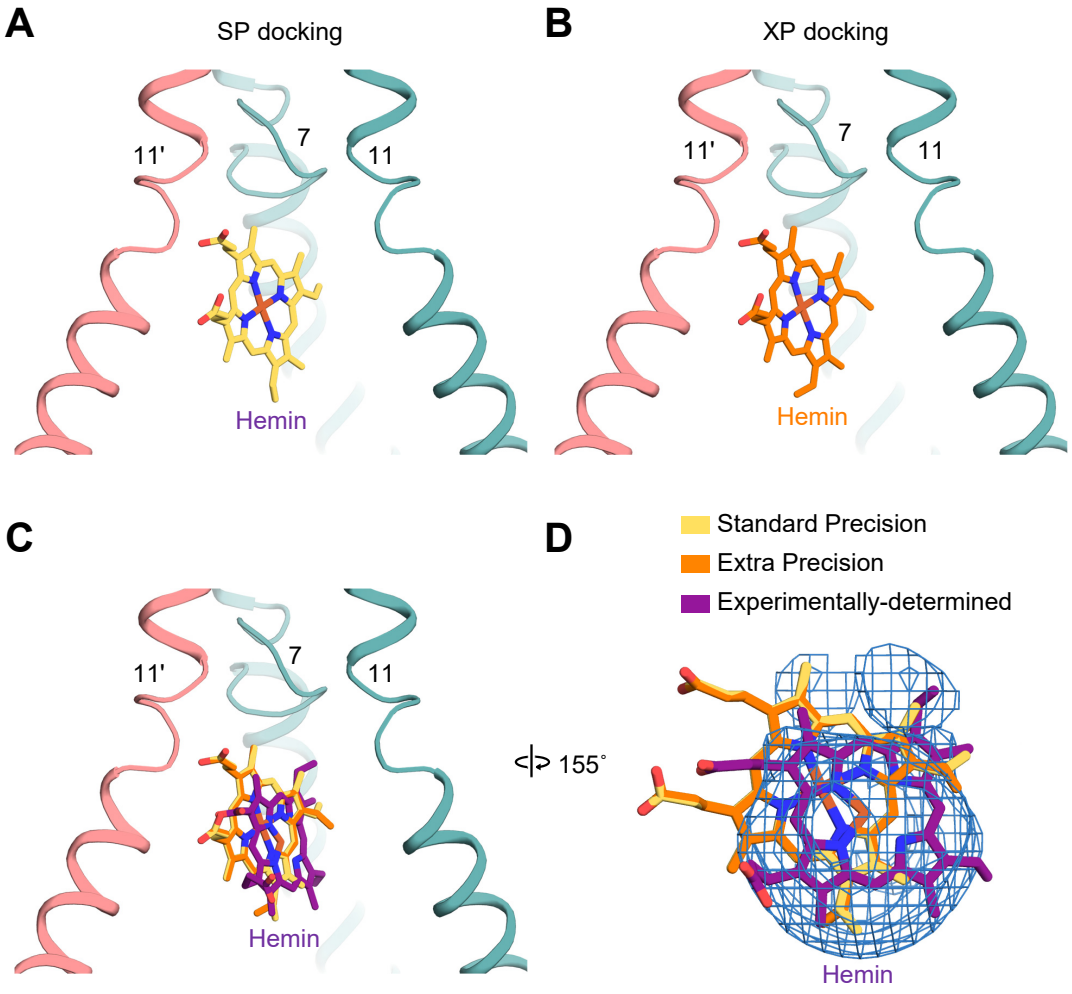

Supplementary Fig. S16. Most favorable binding positions of hemin based on the GLIDE docking method. (A-B) Top-scoring positions from (A) Standard Precision (SP) and (B) Extra Precision (XP) docking analyses for hemin using the ABCB6-ΔTMD0 structure as template. The view is the same as in Figure 5A. The GSHs are omitted for simplicity. (C) The top two positions of hemin are superimposed on the experimentally-determined hemin structure. (D) Superimposition of the experimentally determined structure and *in silico* models. The EM density of hemin (4 σ level) is shown.

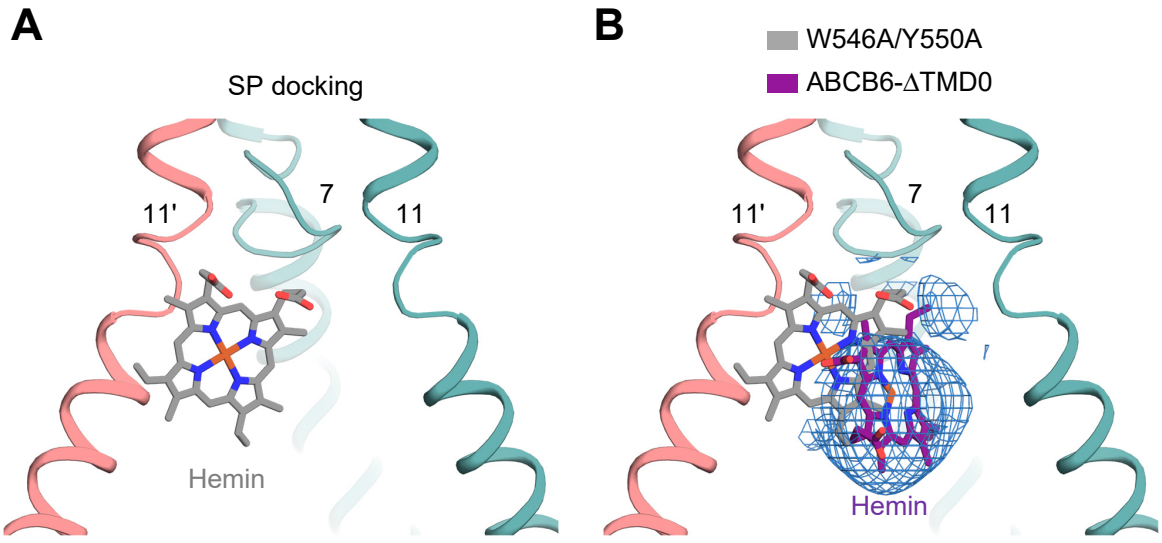

Supplementary Fig. S17. The GLIDE top scoring model of hemin obtained for the W546A/Y550A mutant. (A) Top-scoring position from Standard Precision (SP) docking analysis for hemin using the W546A/Y550A mutant as template. The view is the same as in Figure 5A. The GSHs are omitted for simplicity. (B) Superimposition of the experimentally-determined hemin structure and *in silico* model. The EM density of hemin (4 σ level) is shown.

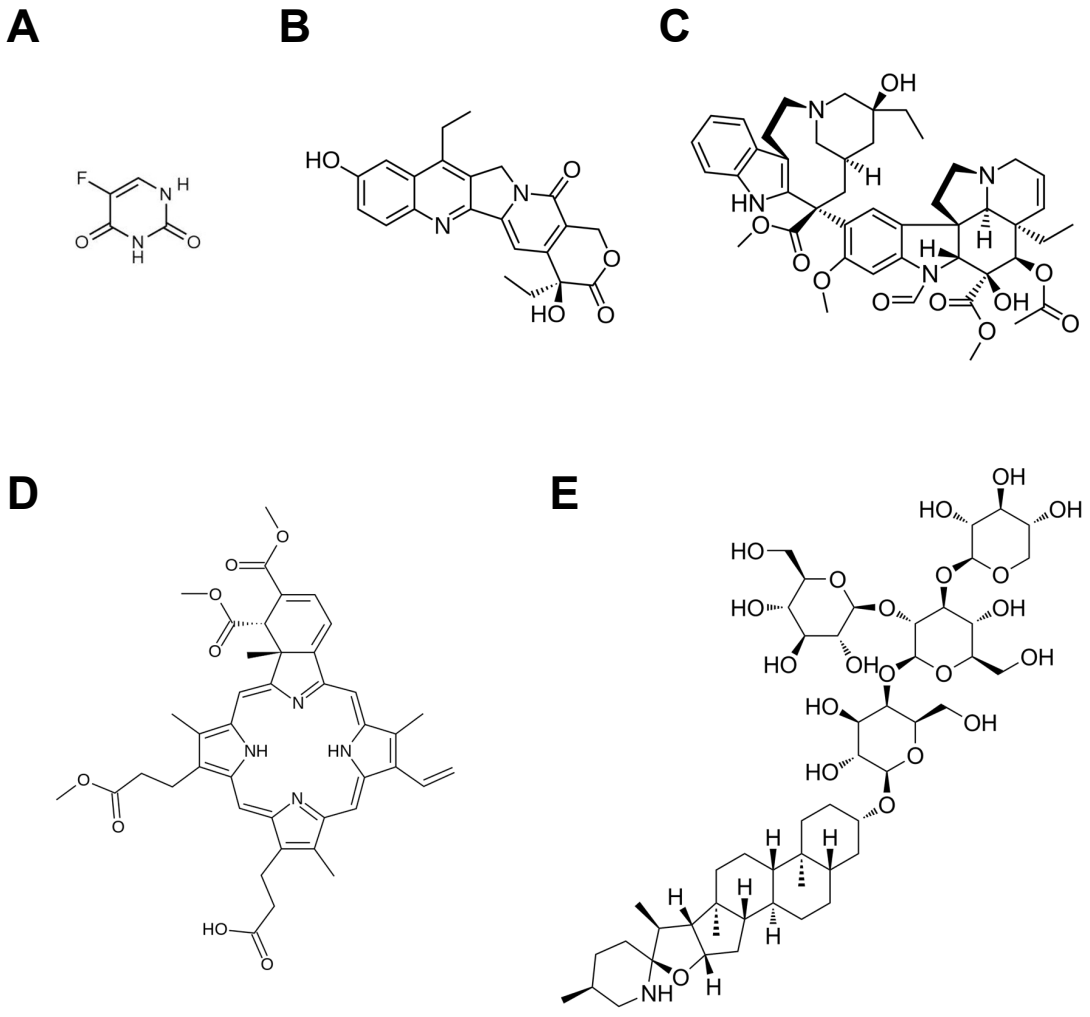

Supplementary Fig. S18. Chemical structures of the various substrates of ABCB6. (A) 5-FU (5-Fluorouracil). (B) SN-38. (C) Vincristine. (D) Verteporfin. (E) Tomatine.

Supplementary Table S1. Cryo-EM data collection, refinement and validation statistics

	Coproporphyrin III EMD-30790 PDB ID 7DNY	**Hemin+GSH** EMD-30791 PDB ID 7DNZ
Data collection and processing		
Magnification	130,000x	100,000x
Voltage (kV)	300	200
Electron exposure (e^{-}/Å^2)	50	50
Defocus range (μm)	-0.8 ~ -2.0	-0.8 ~ -2.6
Pixel size (Super pixel) (Å/pix)	0.656 (0.328)	0.830
Symmetry imposed	C1	C2
Initial particle images (no.)	573,819	852,463
Final particle images (no.)	108,637	283,866
Map resolution (Å)	3.5	3.7
Refinement		
Initial model used (PDB code)	4MRP, 3NH6	7DNY
Map sharpening *B* factor (Å^2)	85.0	178.3
Model composition		
Protein residues (non-H)	8,998	9,338
Ligands (non-H)	223	333
***B* factors (Å^2)**		
Protein	179.4	140.7
Ligand	114.3	114.1
R.m.s. deviations		
Bond lengths (Å)	0.009	0.009
Bond angles (°)	1.222	1.087
Validation		
MolProbity score	1.8	1.7
Clashscore	9.3	6.9
Poor rotamers (%)	1.0	0.6
Ramachandran plot		
Favored (%)	94.5	95.4
Allowed (%)	5.5	4.6
Disallowed (%)	0	0